UCSF
UC San Francisco Previously Published Works

Title

Suppressing APOE4-induced neural pathologies by targeting the VHL-HIF axis.

Permalink

https://escholarship.org/uc/item/9h961018

Journal

Proceedings of the National Academy of Sciences, 122(5)

Authors

Jiang, Wei
Cao, Yiming
Xue, Yue
et al.

Publication Date

2025-02-04

DOI

10.1073/pnas.2417515122

Peer reviewed

eScholarship.org Powered by the California Digital Library
University of California

PNAS RESEARCH ARTICLE | CELL BIOLOGY OPEN ACCESS

Suppressing APOE4-induced neural pathologies by targeting the VHL–HIF axis

Wei I. Jiang[a], Yiming Cao[b], Yue Xue[b], Yichun Ji[b], Benjamin Y. Winer[a,c,d], Rashmi Chandra[a], Xingyuan Fischer Zhang[a], Mengqi Zhang[e], Neel S. Singhal[e], Jonathan T. Pierce[f], Song Chen[b,1], and Dengke K. Ma[a,g,h,1]

Affiliations are included on p. 11.

Edited by Anne C. Hart, Brown University, Providence, RI; received August 29, 2024; accepted December 19, 2024 by Editorial Board Member Yishi Jin

The ε4 variant of human apolipoprotein E (*APOE4*) is a key genetic risk factor for neurodegeneration in Alzheimer's disease and elevated all-cause mortality in humans. Understanding the factors and mechanisms that can mitigate the harmful effects of *APOE4* has significant implications. In this study, we find that inactivating the VHL-1 (Von Hippel–Lindau) protein can suppress mortality, neural and behavioral pathologies caused by transgenic human *APOE4* in *Caenorhabditis elegans*. The protective effects of VHL-1 deletion are recapitulated by stabilized HIF-1 (hypoxia-inducible factor), a transcription factor degraded by VHL-1. HIF-1 activates a genetic program that safeguards against mitochondrial dysfunction, oxidative stress, proteostasis imbalance, and endolysosomal rupture—critical cellular events linked to neural pathologies and mortality. Furthermore, genetic inhibition of *Vhl* reduces cerebral vascular injury and synaptic lesions in *APOE4* mice, suggesting an evolutionarily conserved mechanism. Thus, we identify the VHL–HIF axis as a potent modulator of *APOE4*-induced neural pathologies and propose that targeting this pathway in nonproliferative tissues may curb cellular damage, protect against neurodegeneration, and reduce tissue injuries and mortality.

APOE4 | neurodegeneration | VHL–HIF axis | mitochondrial dysfunction | oxidative stress

Significance

APOE4 encodes a human lipoprotein variant implicated in cholesterol trafficking and metabolism. APOE4 is a major genetic risk factor for age-related Alzheimer's disease (AD) and all-cause mortality in humans, highlighting the importance of understanding APOE4 biology and pathophysiology and identifying targets that can be harnessed to modify APOE4-induced pathologies in cells and organisms. In this study, we demonstrate that targeting *Caenorhabditis elegans* Von Hippel–Lindau (VHL)-1 proteins can markedly suppress neural pathologies, loss of long-lasting behavioral memory, and population mortality induced by transgenic human *APOE4*. Additionally, we present evidence for evolutionarily conserved mechanisms, showing that VHL inactivation strongly mitigates neurovascular injuries and synaptic damage caused by transgenic humanized APOE4 in mice.

Age-related mortality and pathologies occur in nearly all biological species. Understanding the factors that modulate this trajectory is essential for developing strategies to mitigate the impact of aging on population health. Intrinsic genetic determinants and host physiology, extrinsic environmental challenges and abiotic stress, as well as stochastic events all interact to confer mortality risks. In humans, genetic association studies have identified major genetic risk factors for all-cause mortality, including the ε4 allele of the *APOE* gene (*APOE4*) (1–4). This allele also represents the highest genetic risk factor for late-onset Alzheimer's disease (AD) as well as the highest genetic risk modifier of early-onset forms of AD (5–7). Emerging human studies implicate *APOE4* homozygosity as a major genetic cause, not just a risk modifier, of AD that constitutes one of the most frequent human Mendelian disorders (8). APOE4 proteins differ in cholesterol transport capabilities compared to its allelic counterparts, and, contrary to its heightened association with AD risk, it is linked to decreased susceptibility to age-related macular degeneration (9–11). Genetic variations including non-*APOE4* variant alleles of *APOE* have also been shown to be associated with reduced mortality in rare long-lived human centenarians (12). *APOE4* may increase AD risk through a gain of abnormal function, with APOE loss-of-function variant carriers showing resilience to cognitive decline and AD pathology (13). These studies have provided intriguing cases of how genetic variations may link to mortality and age-related diseases and AD in humans. However, despite these advances, establishing causal and mechanistic relationships among genetic variations, cellular processes, environmental impacts, and mortality rates remains a formidable challenge.

To identify causal genetic factors that drive or modify age-related neurodegeneration and mortality and to elucidate their underlying mechanisms, the nematode *Caenorhabditis elegans* represents a well-suited model organism (14–17). Its amenability to genetic manipulation, short lifespan, and well-characterized genome provide an ideal platform for discovering novel genetic modifiers of age-related mortality and pathologies within the context of a whole organism and with well-controlled environmental conditions (17–19). In addition, the relatively simple and transparent anatomy of *C. elegans* allows for direct observation of cellular and physiological changes throughout its lifecycle, facilitating the identification of cellular mechanisms and their impact on mortality and pathologies. Pioneering investigations of longevity mutants in *C. elegans* have underscored the importance of the insulin, PI3K, and the mechanistic target of TOR (mTOR) pathways, leading to discoveries of their evolutionarily conserved roles regulating key aging processes and

Author contributions: W.I.J., Y.C., Y.X., Y.J., S.C., and D.K.M. designed research; W.I.J., Y.C., Y.X., Y.J., R.C., and X.F.Z. performed research; W.I.J., Y.C., Y.X., Y.J., B.Y.W., R.C., M.Z., N.S.S., J.T.P., and S.C. contributed new reagents/analytic tools; W.I.J., Y.C., Y.X., Y.J., B.Y.W., R.C., S.C., and D.K.M. analyzed data; and W.I.J., J.T.P., S.C., and D.K.M. wrote the paper.

The authors declare no competing interest.

This article is a PNAS Direct Submission A.C.H. is a guest editor invited by the Editorial Board.

Copyright © 2025 the Author(s). Published by PNAS. This open access article is distributed under Creative Commons Attribution-NonCommercial-NoDerivatives License 4.0 (CC BY-NC-ND).

[1]To whom correspondence may be addressed. Email: ChenS@cpu.edu.cn or Dengke.Ma@ucsf.edu.

This article contains supporting information online at https://www.pnas.org/lookup/suppl/doi:10.1073/pnas.2417515122/-/DCSupplemental.

Published January 28, 2025.

age-related pathologies across various eukaryotic organisms, including humans (20–22). Besides the trajectory of aging under normal culture conditions, *C. elegans* is also subject to rapidly increased mortality when exposed to severe environmental stresses, including elevated temperature, pathogen infection, and abiotic stress (17, 23, 24). While mild stress can extend longevity through the mechanism of hormesis, it remains largely unknown how mortality accelerates when *C. elegans* is severely stressed (17, 23, 25, 26).

Genetic studies in *C. elegans* have identified reduction- or loss-of-function (LOF) alleles, including those of *daf-2* and *vhl-1*, which can extend longevity and confer broad stress resilience (27–30). *daf-2* encodes a homolog of insulin receptors that orchestrate anabolic metabolism, autophagy regulation, and somatic maintenance program during aging. *daf-2* mutants are exceptionally long lived and stress resistant. *vhl-1*, the ortholog of the Von Hippel–Lindau tumor suppressor gene, encodes an E3-ubiquitin ligase that targets the hypoxia-inducible factor HIF-1 for degradation. Loss of Von Hippel–Lindau (VHL)-1 stabilizes HIF-1 and activates a genetic program linked to both longevity extension and stress resilience. While HIF-activating VHL mutations in humans increase risks to various cancers, including clear cell renal cell carcinoma, HIF, and its target gene activation in nonproliferative cells, such as neurons and cardiomyocytes, can be protective against ischemic insults, reperfusion injuries, and metabolic stress (31–33). Although previous transcriptomic and proteomic studies unveiled many transcriptional targets of HIF, specific mechanisms underlying the protective effect of the VHL–HIF axis in the context of neural pathologies, organismal stress resilience, and longevity still remain unclear.

In light of the escalating mortality rates associated with aging and exacerbated by diverse intrinsic and extrinsic factors, our study aimed to identify factors and mechanisms capable of mitigating these outcomes. We find that *vhl-1* loss or stabilized HIF-1-regulates genes that contribute to guarding against cellular processes mechanistically linked to APOE4-induced neural pathologies and mortality in *C. elegans*. We further used *APOE4*-humanized mice to show the evolutionarily conserved action of VHL inhibition in mitigating APOE4-induced tissue injury and neural pathologies.

Results

Roles of VHL-1 in Suppressing Mortality. We showed previously that transgenic gain-of-function neuronal expression of human *APOE4 (vxIs824)* in *C. elegans* specifically exacerbated neurodegeneration (34). To study potential effects of APOE4 on neural pathologies and mortality using a fast, reproducible, and robust model, we examined the mortality trajectory (lifespan curve) of *APOE4*-transgenic *C. elegans* under various constant conditions of temperature stress beyond the normal range (15 °C to 25 °C). When subjected to a constant temperature of 28 °C, wild-type (WT) animals died within a few days (median lifespan of 4 d post-L4), whereas neuronal *APOE4* expression drastically shortened the lifespan (median lifespan fewer than 2 d post-L4) (Fig. 1*A*). Under such constant heat stress, *APOE4* expression also led to profound morphological deterioration of the PVD neuron (Fig. 1*B*).

Elevated temperature stress causes increased levels of ROS and HIF-1 activation in *C. elegans* (35, 36). Loss of VHL-1 leads to the stabilization of HIF-1, providing a defense mechanism against hypoxic and oxidative stresses (Fig. 1*C*). As we previously discovered that VHL-1 inactivation mitigates the morphological degeneration of dopaminergic neurons in *C. elegans* complex I mutants (37), we examined how a *vhl-1(ok161)* deletion allele affected the mortality of *APOE4*-transgenic *C. elegans* under 28 °C. We found that *vhl-1* deletion abolished the effect of *APOE4* on increased mortality under 28 °C and extended lifespan in WT animals under 28 °C (Fig. 1*D*). These results establish a *C. elegans* model for rapid APOE4-induced mortality and identified potent mortality-suppressing effects of *vhl-1(ok161)* LOF mutations.

APOE4 represents a lipoprotein variant characterized by a diminished capacity for lipid recycling, resulting in intracellular accumulation of cholesterol that is highly susceptible to oxidation (38–40). Because *C. elegans* cannot synthesize cholesterol, its cholesterol levels are determined, and can be controlled, by its diet. We developmentally synchronized and cultured the *APOE4(vxIs824)*-transgenic strain on culture plates deficient in exogenous cholesterol (*SI Appendix*, Fig. S1*A*), a procedure to reduce overall cholesterol intake during larval development (41). Such cholesterol-reduction conditions markedly restored the lifespan of *APOE4*-transgenic animals, without affecting that of wild type (Fig. 1*E*) or the mortality-decreasing effect of *vhl-1(ok161)* deletion (Fig. 1*F*). Exogenous supplementation with N-acetyl-cysteine (NAC), a precursor of glutathione and scavenger of ROS previously used and validated in *C. elegans* (42–45), dose-dependently suppressed the mortality effect of APOE4 (Fig. 1 *G* and *H*), suggesting causal effects of oxidative stress. We also observed that body size was reduced in *APOE4*-transgenic *C. elegans* when compared to wild type at normal 20 °C, while *vhl-1(ok161)* deletion mutation or reduction of cholesterol uptake starting at embryonic stages was sufficient to rescue body sizes (*SI Appendix*, Fig. S1 *B* and *C*).

We used a heat-independent approach to generate excessive oxidative stress based on a transgenic strain with blue light-induced production of superoxide from neuronal expression of a genetically encoded miniSOG transgene (46, 47). We observed that blue light exposure in this strain induced a rapid and robust increase of population mortality that was strongly suppressed by dietary cholesterol reduction or NAC supplementation (Fig. 1*I*). *vhl-1(ok161)* deletion recapitulated such mortality-suppressing effects (Fig. 1*J*). Furthermore, we found that *APOE4(vxIs824)* also increased the mortality of *C. elegans* under 20 °C normal culture conditions and *vhl-1(ok161)* deletion or cholesterol reduction strongly suppressed the mortality effect of *APOE4* (Fig. 1 *K* and *L* and *SI Appendix*, Fig. S1*D*).

Taken together, these results identify VHL-1 as a potent modifier of APOE4 in mortality and suggest that *APOE4* expression may cause abnormal accumulation or distribution of intracellular cholesterol, oxidation of which by ROS contributes to an increase in population mortality suppressible by *vhl-1* deletion.

Roles of HIF-1 in Suppressing Mortality Caused by APOE4. We next examined roles of HIF-1 in suppressing mortality. We monitored hypoxic and redox stress responses using the well-characterized HIF-1-dependent transcriptional reporter, *cysl-2p::Venus* (48–50). As would be predicted for stabilized HIF-1, *vhl-1* deletion strongly activated *cysl-2p::Venus* in a HIF-dependent manner (Fig. 2 *A* and *B* and *SI Appendix*, Fig. S2*A*). Under normal 21% oxygen conditions, elevated temperature at 28 °C caused a time- and temperature-dependent activation of *cysl-2p::Venus* (*SI Appendix*, Fig. S2 *B* and *C*), consistent with elevated oxidative stress and HIF-1 activation by heat (35). LOF *hif-1* fully suppressed the mortality-reducing effects of *vhl-1* under both normal culture conditions (29, 51) and on *APOE4* at 28 °C (Fig. 2 *A* and *C*). We further characterized the effects of a stabilized form of HIF-1 using a transgene *otIs197* that expresses a nondegradable (VHL-resistant) P621A variant and driven by the *unc-14* promoter (52) (Fig. 2*D*). Testing thermal stress, we found that stabilized

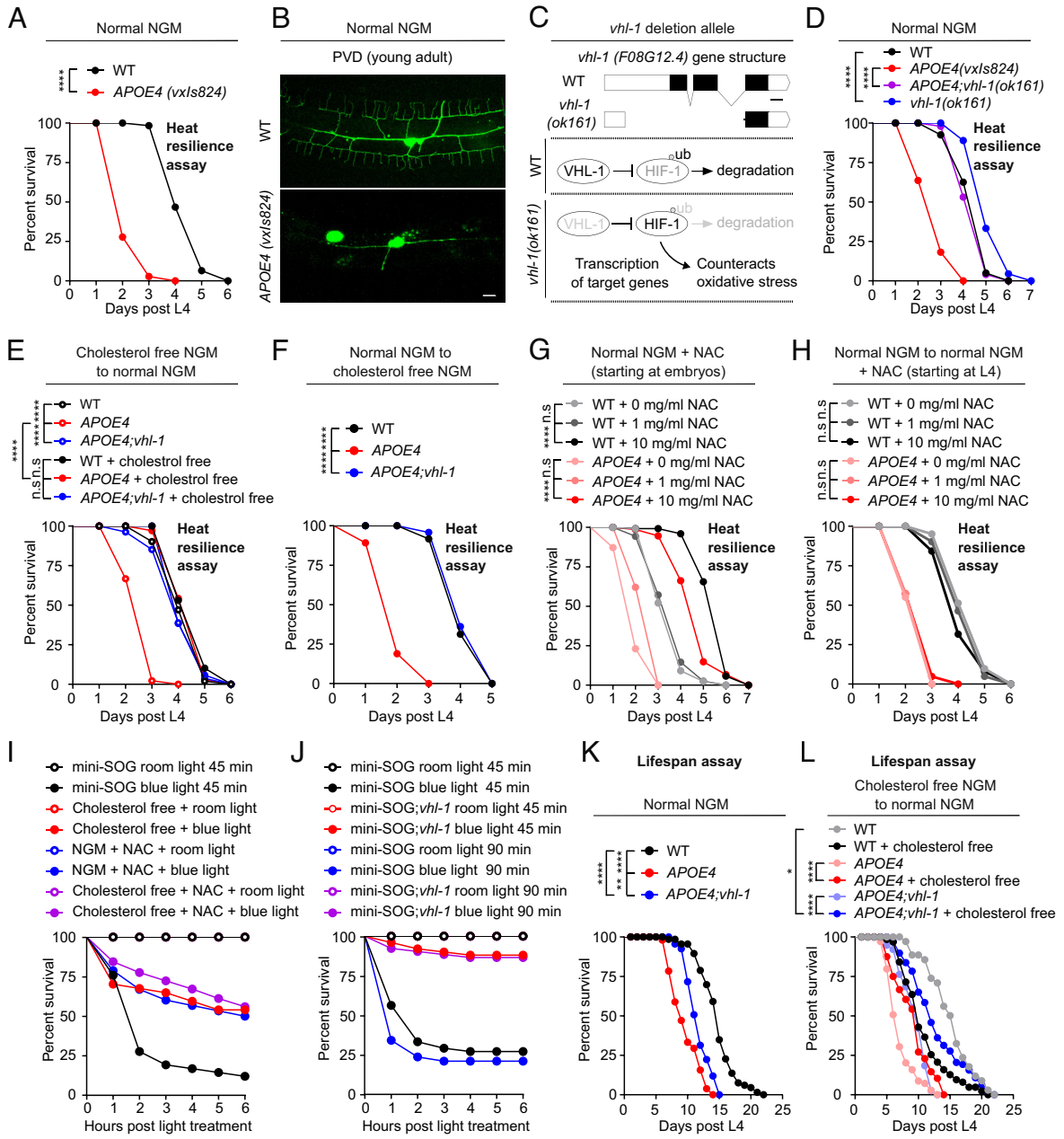

Fig. 1. Loss of *vhl-1* suppresses neural pathologies and mortality induced by oxidative stress–causing factors (miniSOG, heat, and *APOE4*). (*A*) Lifespan curves of N2 WT and pan-neuronal *APOE4(vxIs824)* transgenic animals at 28 °C starting at L4 on normal NGM, showing a 50% median and 50% maximal survival decrease in *APOE4(vxIs824)* compared to WT. **** indicates $P < 0.0001$ (WT: n = 62 animals, *APOE4*: n = 36 animals). (*B*) Representative confocal microscopic images of PVD neurons (*wyIs592[ser-2prom-3p::myr-GFP]*) in WT and pan-neuronal *APOE4(vxIs824)* animals at the young adult stage on normal NGM, showing PVD abnormalities with an apparent loss of third and fourth branches. (Scale bar: 10 μm.) (*C*) Schematic of the *vhl-1(ok161)* loss-of-function deletion allele (with exons 2 and 3 deleted) that leads to impaired ubiquitination and stabilized HIF-1 to counteract oxidative stress. (Scale bar: 100 bp.) (*D*) Lifespan curves of WT, pan-neuronal *APOE4(vxIs824)*, *vhl-1(ok161)* mutants, and *APOE4(vxIs824); vhl-1(ok161)* animals at 28 °C starting at L4 on normal NGM. **** indicates $P < 0.0001$ [WT: n = 40 animals, *APOE4*: n = 44 animals, *APOE4(vxIs824); vhl-1(ok161)*: n = 49 animals, *vhl-1(ok161)*: n = 45 animals]. (*E*) Lifespan curves of WT, *APOE4(vxIs824)*, and *APOE4(vxIs824); vhl-1(ok161)* animals with or without early-life cholesterol-free NGM (starting at embryos) to L4 on cholesterol-free NGM, followed by picking to normal NGM and culturing at 28 °C. **** indicates $P < 0.0001$; n.s. indicates nonsignificant [WT: n = 51 animals, *APOE4(vxIs824)*: n = 45 animals, *APOE4(vxIs824); vhl-1(ok161)*: n = 54 animals, WT + cholesterol-free: n = 49 animals, *APOE4(vxIs824)* + cholesterol-free: n = 35 animals, *APOE4(vxIs824); vhl-1(ok161)* + cholesterol-free: n = 52 animals]. (*F*) Lifespan curves of WT, *APOE4(vxIs824)*, and *APOE4(vxIs824); vhl-1(ok161)* grown to L4 on normal NGM, followed by picking to cholesterol-free NGM and culturing at 28 °C. **** indicates $P < 0.001$ [WT: n = 48 animals, *APOE4(vxIs824)*: n = 37 animals, *APOE4(vxIs824); vhl-1(ok161)*: n = 47 animals]. (*G*) Lifespan curves of WT and *APOE4(vxIs824)* starting from early life (embryos) with the indicated NAC diet concentrations (0 mg/mL, 1 mg/mL, and 10 mg/mL) to L4 on normal NGM supplemented with the indicated NAC concentration, followed by picking to normal NGM supplemented with the indicated concentration of NAC and culturing at 28 °C. **** indicates $P < 0.001$; n.s. indicates nonsignificant [WT + 0 mg/mL: n = 340 animals, WT + 1 mg/mL: n = 357 animals, WT + 10 mg/mL: n = 122 animals, *APOE4(vxIs824)* + 0 mg/mL: n = 78 animals, *APOE4(vxIs824)* + 1 mg/mL: n = 29 animals, *APOE4(vxIs824)* + 10 mg/mL: n = 74 animals]. (*H*) Lifespan curves of WT and *APOE4(vxIs824)* grown to L4 on normal NGM, followed by picking to normal NGM supplemented with the indicated concentration of NAC (starting at L4) and transferred to 28 °C. *** indicates $P < 0.001$; n.s. indicates nonsignificant (n > 40 animals per condition). (*I*) Percent survival of miniSOG animals *[unc-25p::tomm20::miniSOG::SL2::RFP]*, grown to L4 starting at early life (embryos) with NAC supplement, starting at early life (embryos) with cholesterol-free NGM, or normal NGM, followed by room light or blue light treatments for 45 min (n > 40 animals per condition). (*J*) Percent survival of miniSOG animals *[unc-25p::tomm20::miniSOG::SL2::RFP]* or LOF mutant *vhl-1(ok161)*; miniSOG animals grown to L4 on normal NGM, followed by room light or blue light treatments for 45 min or 90 min (n > 40 animals per condition). (*K*) Lifespan curves of WT, *APOE4(vxIs824)*, and *APOE4(vxIs824); vhl-1(ok161)* animals at constant 20 °C on normal NGM. ** indicates $P < 0.01$; **** indicates $P < 0.0001$ (n > 40 animals per condition). (*L*) Lifespan curves of WT, *APOE4(vxIs824)*, and *APOE4(vxIs824); vhl-1(ok161)* animals with or without (starting at embryos) cholesterol diet to L4, followed by picking to normal NGM and culturing at 20 °C. * indicates $P < 0.05$; **** indicates $P < 0.0001$ (n > 40 animals per condition).

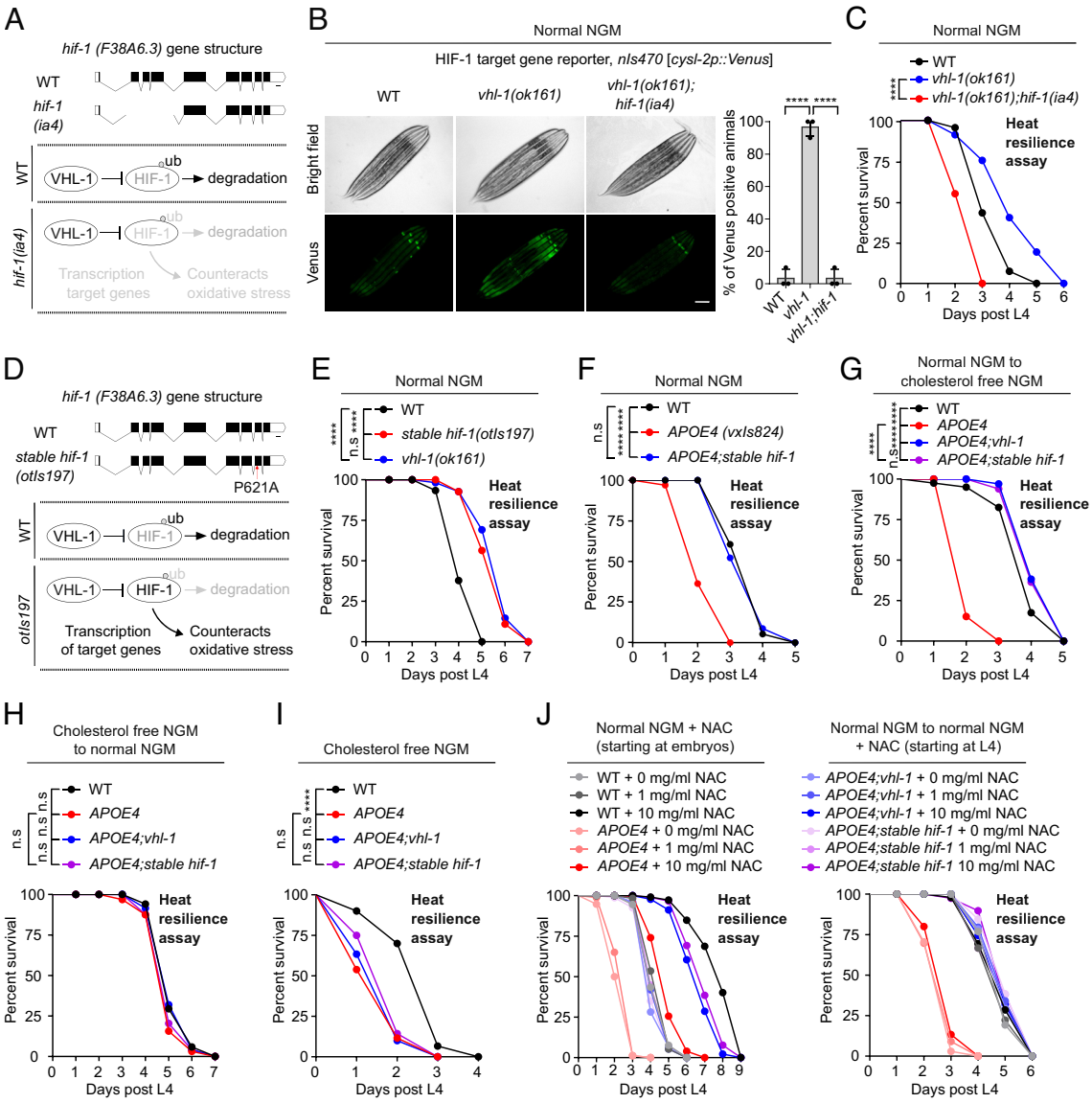

Fig. 2. Stabilized HIF-1 recapitulates the effects of VHL-1 inactivation. (*A*) Schematic of the *hif-1(ia4)* LOF deletion allele (1,231 bp deletion of the second, third, and fourth exons) and its impaired capacity to counteract oxidative stress. (Scale bar: 100 bp.) (*B*) Representative epifluorescence images and quantification showing that *cysl-2p::Venus* constitutive upregulation in *vhl-1(ok161)* LOF mutants is blocked by *hif-1(ia4)* LOF mutants. (Scale bar: 100 μm.) **** indicates $P < 0.0001$ (n > 30 animals per condition). (*C*) Lifespan curves of WT, *vhl-1(ok161)* LOF mutants, and *vhl-1(ok161); hif-1(ia4)* double LOF mutant animals at 28 °C starting at L4 on normal NGM. **** indicates $P < 0.0001$ (n > 40 animals per condition). (*D*) Schematic of the nondegradable form of HIF-1 (P621A) expressed by the unc-14 promoter (predominantly active in neurons) in a *hif-1* mutant background (*otIs197 [unc-14p::hif-1(P621A) + ttx-3p::RFP]*). (Scale bar: 100 bp.) (*E*) Lifespan curves of WT, nondegradable form of HIF-1 (P621A) *(otIs197)*, or *vhl-1(ok161)* LOF mutant animals at 28 °C starting at L4 on normal NGM. **** indicates $P < 0.0001$; n.s. indicates nonsignificant (n > 40 animals per condition). (*F*) Lifespan curves of WT, *APOE4(vxIs824);* HIF-1 (P621A) *(otIs197)*, and *APOE4(vxIs824)* animals at 28 °C starting at L4 on normal NGM. **** indicates $P < 0.0001$; n.s. indicates nonsignificant (n > 40 animals per condition). (*G*) Lifespan curves of WT, *APOE4(vxIs824)*, *APOE4(vxIs824); vhl-1(ok161)*, and *APOE4(vxIs824); HIF-1 (P621A) (otIs197)* animals grown to L4 on normal NGM, followed by picking to cholesterol-free NGM and culturing at 28 °C. *** indicates $P < 0.001$; n.s. indicates nonsignificant (n > 40 animals per condition). (*H*) Lifespan curves of WT, *APOE4(vxIs824)*, *APOE4(vxIs824); vhl-1(ok161)*, and *APOE4(vxIs824); HIF-1 (P621A) (otIs197)* animals starting at early life (embryos) with cholesterol-free NGM to L4, followed by picking to normal NGM and culturing at 28 °C. n.s. indicates nonsignificant (n > 40 animals per condition). (*I*) Lifespan curves of WT, *APOE4(vxIs824)*, *APOE4(vxIs824); vhl-1(ok161)*, and *APOE4(vxIs824); HIF-1 (P621A) (otIs197)* animals starting at early life (embryos) with cholesterol-free NGM to L4, followed by picking to cholesterol-free NGM and culturing at 28 °C. **** indicates $P < 0.0001$; n.s. indicates nonsignificant (n > 40 animals per condition). (*J*) Lifespan curves of WT, *APOE4(vxIs824)*, *APOE4(vxIs824); vhl-1(ok161)*, and *APOE4(vxIs824); HIF-1 (P621A) (otIs197)* animals starting at early life (embryos) with the indicated NAC concentration diet to L4 on normal NGM, followed by picking to normal NGM supplemented with the indicated concentration of NAC and transferred to 28 °C (*Left*). Lifespan curves of WT, *APOE4(vxIs824)*, and *APOE4(vxIs824); stable hif-1 (otIs197)* animals grown to L4 on normal NGM, followed by picking to normal NGM supplemented with the indicated concentration of NAC (starting at L4 stage) and culturing at 28 °C (*Right*). (n > 40 animals per condition).

HIF-1(*otIs197)* extended the lifespan of wild type grown at 28 °C (Fig. 2*E*) and suppressed the mortality effect of *APOE4(vxIs824)* to the same level as *vhl-1* deletion (Fig. 2*F*). Testing cholesterol as a stressor, we found that reducing cholesterol during larval development but not during adult stage occluded negative effects of APOE4 in both wild type and stabilized HIF-1 transgenic animals (Fig. 2 *G–I*). In addition, supplementation with NAC dose-dependently reduced mortality of APOE4 but to a lesser extent in stabilized HIF-1(*otIs197*) or *vhl-1* deletion mutant animals (Fig. 2*J*). Furthermore, stabilized HIF-1(*otIs197*) also recapitulated the effect of *vhl-1* deletion on reducing the mortality of *APOE4* transgenic animals at 20 °C (*SI Appendix*, Fig. S2 *D–G*).

To test whether HIF-1 played a similar role beyond *C. elegans*, we generated a HEK293T cell line by expressing stabilized HIF-1 by lentiviral infection (*SI Appendix*, Fig. S2*H*). We found that it similarly protected HEK293T cells against thermal stress

conditions and suppressed the mortality-increasing effect of APOE4 (*SI Appendix*, Fig. S2*I*). The abundance, subcellular localization, or secretion of APOE4 was not affected by stabilized HIF-1 or thermal stress in HEK293T cells (*SI Appendix*, Fig. S2 *J* and *K*). Exogenous supplementation with *APOE4*-expressing HEK293T cell supernatants did not affect the mortality of *C. elegans* under 28 °C (*SI Appendix*, Fig. S2*L*).

Together, these results demonstrate roles of HIF-1 in mediating effects of *vhl-1* loss in mortality and that a stabilized HIF-1 transgene is sufficient to suppress APOE4-induced increase in mortality during normal aging and under heightened heat stress conditions.

Cellular Consequences of APOE4 Suppressed by *vhl-1* Loss or HIF-1 Activation. To understand mechanisms of APOE4 toxicities and protection by *vhl-1* and HIF-1, we assessed the molecular and cellular abnormalities in neuronal *APOE4(vxIs824)* transgenic animals. To identify pathways potentially dysregulated by APOE4, we performed bulk transcriptome profiling. RNAseq analysis revealed that APOE4 caused numerous alterations in genes involved in stress responses and proteostasis (*SI Appendix*, Fig. S3 *A–D*). To monitor proteostasis in vivo, we generated a transcriptional reporter for the heat shock protein-encoding *hsp-16.2* as a live indicator. We found that *hsp-16.2p::GFP* remained at low baseline levels throughout development in the wild type under normal culture conditions (Fig. 3*A* and *SI Appendix*, Fig. S4*A*). By comparison, APOE4 increased *hsp-16.2p::GFP* expression dramatically starting at the fourth larval stage and with the highest penetrance at day 5 post-L4 (Fig. 3 *A* and *B*). APOE4 elevated proteostatic stress, as revealed by this reporter, even without exogenous proteostasis-perturbing conditions, such as heat stress. High-magnification confocal microscopic analysis revealed the site of abnormally up-regulated *hsp-16.2*p::GFP expression predominantly in the body wall muscle, while its expression in a few unidentified neurons remained largely unaltered (Fig. 3 *C–E*). As a more direct readout of proteostasis (53), we also monitored length-dependent aggregation of polyglutamine(polyQ)-YFP fusion proteins in *C. elegans*. We found that APOE4 increased *unc-54p::Q40::YFP* (40 polyQ repeats) aggregation, but not shorter repeats of *unc-54p::Q35::YFP* (35 polyQ repeats) in the body wall muscle (Fig. 3*F* and *SI Appendix*, Fig. S3 *B* and *C*). To monitor the proteotoxic consequences of APOE4 and *vhl-1*, we used Western blot to assess oxidative stress-induced actin cleavage (Fig. 3*G*). While APOE4 caused dramatic accumulation of actin species with lower molecular weight indicative of protein cleavage, such proteotoxic effects were largely absent in *vhl-1* LOF deletion mutants or stabilized HIF-1(*otIs197)* animals carrying APOE4 (Fig. 3*G*). Actin cleavage also occurred in WT animals subjected to 28 °C heat stress and was similarly suppressed in *vhl-1* deletion mutants or stabilized HIF-1*(otIs197)* animals without APOE4 (Fig. 3*G*). Immunocytochemistry showed that the antibody used for actin stained mostly body wall muscles, consistent with *hsp-16.2p::GFP* activation in the same tissue (Fig. 3*H*). Given neuronal-specific APOE4 expression, these results suggest non-cell-autonomous proteotoxic effects of APOE4 suppressible by *vhl-1* loss or HIF-1 activation.

We next examined potential consequences of APOE4 with respect to *vhl-1* and HIF in neurons. Given the dramatic morphological deterioration of the PVD neuron in APOE4 animals (Fig. 1*B* and *SI Appendix*, Fig. S5 *A–D*), we focused on a detailed longitudinal analysis of PVD morphological integrity in both *APOE4(vxIs824)* and *APOE4(vxIs824)*; *vhl-1(ok161)* animals. Confocal imaging analysis revealed that the morphological defect, including decreased dendrite numbers and complexity, of the PVD neuron manifested early in the fourth larval stage and persisted throughout adulthood (*SI Appendix*, Fig. S5 *A–C*). We found that *vhl-1* deletion strongly suppressed the morphological defects of the PVD neuron in neuronal APOE4 transgenic animals (Fig. 4 *A–C*). While APOE4 caused a nearly fully penetrant defect of PVD neurons at the larval L4 stage, *vhl-1* mutants exhibited marked suppression of defects in all three stages examined (Fig. 4 *D–F*). Together, these results show that APOE4 can cause both non-cell-autonomous and cell-autonomous cellular defects, both of which are suppressible by *vhl-1* LOF.

In addition, we asked whether pan-neuronal expression of *APOE4* causes behavioral learning defects and memory loss in *C. elegans* and whether such behavioral defects could also be rescued by *vhl-1* LOF. To address these questions, we used a spaced, repeated conditioning paradigm (Fig. 4*G*) in which *C. elegans* learns and remember to avoid butanone (54, 55), an innately attractive odor released by nutritious bacteria. We found that *APOE4* does not appear to affect initial attraction to butanone and avoidance learning, as quantified using a chemotaxis index (Fig. 4*H*). However, *APOE4(vxIs824)* specifically and strongly decreased memory retention at 16 h posttraining (Fig. 4*I*). Similar to rescue of PVD morphology, *vhl-1* deletion markedly restored the *APOE4*-induced loss of long-lasting memory (Fig. 4 *H* and *I*). These results highlight the pathological role of *APOE4* in causing behavioral memory loss in *C. elegans* and demonstrate that *vhl-1* deletion functionally rescues *APOE4*-induced memory loss.

To further investigate cellular mechanisms underlying the neuronal toxicity of APOE4 and protection by *vhl-1* or HIF-1, we examined major organelles in live neurons, including mitochondria, lysosomes, and endosomes. Using the neuronal organelle-specific fluorescent markers (schematic in *SI Appendix*, Fig. S6*A*) for longitudinal imaging, we found that APOE4 caused a striking age-dependent increase of the fluorescent marker for mitochondria (Fig. 5 *A* and *B*) and decrease of the fluorescent marker for lysosomes (Fig. 5 *C* and *D*). The increase of mitochondrial markers did not manifest until the fourth larval stage and persisted throughout the adult stage (Fig. 5*B*). The changes in organelle reporters could not be explained by APOE4 affecting transgene expression since RNAseq results (*SI Appendix,* Fig. S3 *A–D*) indicated that APOE4 does not affect the expression of *ric-19*, the promoter of which drives the organelle markers. Strikingly, *vhl-1* deletion or stabilized HIF-1 strongly suppressed the abnormally increased mitochondrial markers by APOE4 (Fig. 5 *E* and *F*). APOE4 did not appear to affect non-neuronal mitochondria or neuronal endosomes (*SI Appendix*, Fig. S6 *B–D*). Reduction of cholesterol also suppressed the effect of APOE4 on such mitochondrial and lysosomal phenotypes (*SI Appendix*, Fig. S6 *E–G*). These results reveal organelle-specific defects caused by APOE4 and suggest that APOE4 possibly exerts cellular toxicity through excess cholesterol, oxidation of which leads to lysosomal membrane disruption, impaired mitophagy, and mitochondria clearance, defects suppressible by *vhl-1* inhibition and HIF-1 activation.

Transcriptional Targets of HIF-1 Mediating Effects of *vhl-1* and HIF-1. We aimed to determine the transcriptional targets of HIF-1 and their mechanisms of action underlying protection against heat stress and APOE4. Proteomic and transcriptomic studies have identified many genes differentially regulated in *vhl-1* mutants (56–58). We used qRT-PCR and GFP reporters to validate many of these targets based on their dramatic upregulation in *vhl-1(ok161)* mutants grown at 28 °C, under which condition HIF-1 is both stabilized and activated in target gene transcriptional transactivation (Fig. 6*A*). We used deletion mutants or RNA interference (RNAi) (when deletion mutants were not available)

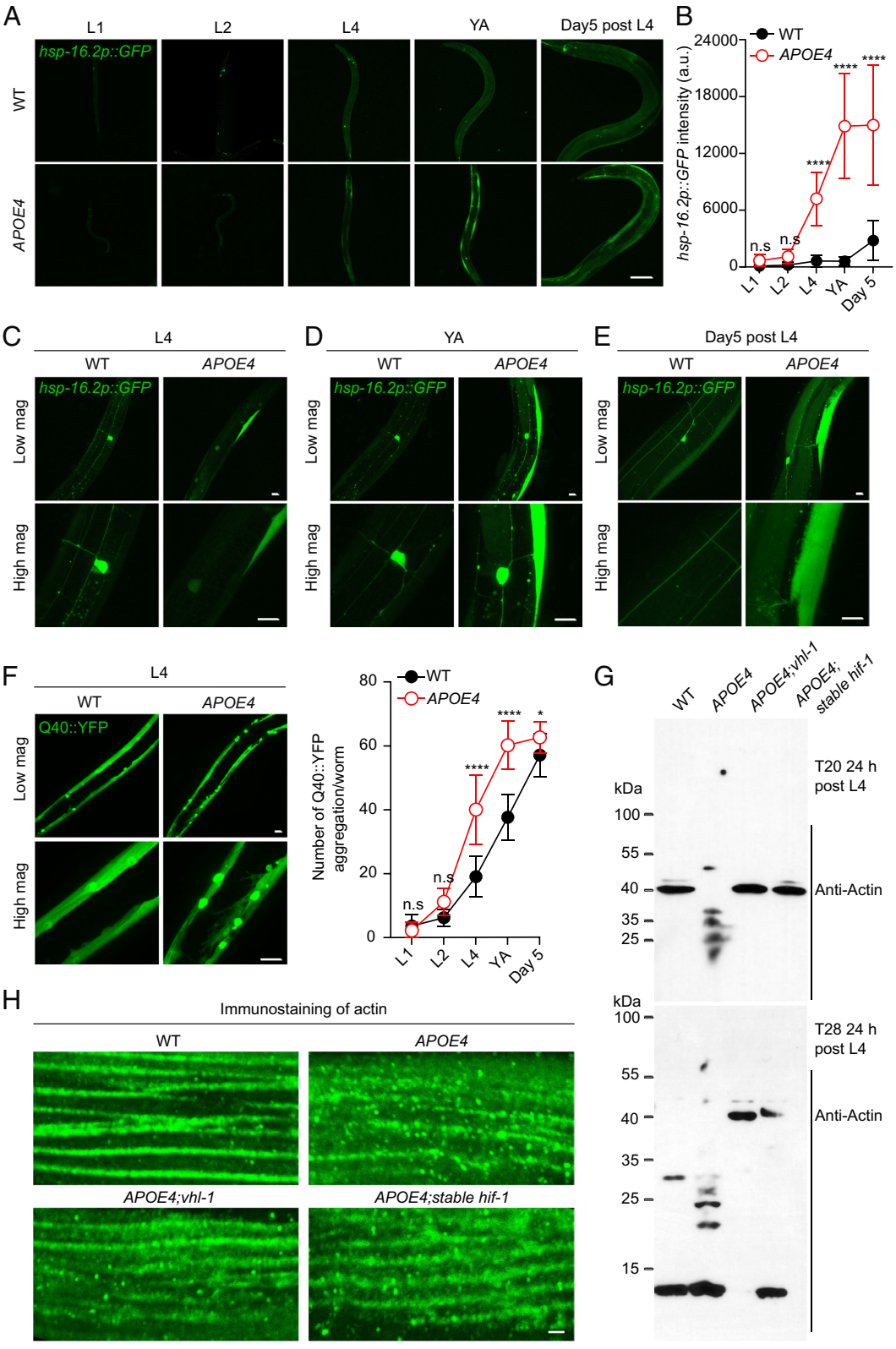

Fig. 3. *APOE4* causes non-cell-autonomous proteostasis dysregulation and actin cleavage suppressed by *vhl-1*. (*A*) Representative confocal low-magnification images of *hsp-16.2p::GFP* in body wall muscles in WT and *APOE4 (vxIs824)* animals at different stages of L1, L2, L4, young adult (day 1 post-L4), and Day 5 post-L4 on normal NGM. (Scale bar: 100 μm.) (*B*) Quantification of fluorescence intensities of *hsp-16.2p::GFP* in body wall muscles under conditions indicated. *** indicates $P < 0.001$; n.s. indicates nonsignificant (n > 30 animals per condition). (*C–E*) Representative confocal high-magnification images of *hsp-16.2p::GFP* in body wall muscles in WT and *APOE4 (vxIs824)* at different stages of L4, young adult (day 1 post-L4), and Day 5 post-L4 on normal NGM. (Scale bar: 10 μm.) (*F*) Representative confocal high-magnification images of *unc-54p::Q40::YFP* in body wall muscles in WT and *APOE4 (vxIs824)* at stages of L4 on normal NGM, and quantification of aggregation number of *unc-54p::Q40::YFP* in body wall muscles under conditions indicated. (Scale bar: 10 μm.) * indicates $P < 0.05$, **** indicates $P < 0.0001$, and n.s. indicates nonsignificant (n > 30 animals per condition). (*G*) Representative SDS-PAGE western blots of WT, *APOE4(vxIs824)*, *APOE4(vxIs824); vhl-1(ok161)*, and *APOE4(vxIs824); HIF-1 (P621A) (otIs197)*. (*H*) Representative confocal high-magnification images in body wall muscles of WT, *APOE4(vxIs824)*, *APOE4(vxIs824); vhl-1(ok161)*, and *APOE4(vxIs824); HIF-1 (P621A) (otIs197)* animals immunostained with primary antibody against actin at young adult stages (24 h post-L4) on normal NGM. (Scale bar: 1 μm.)

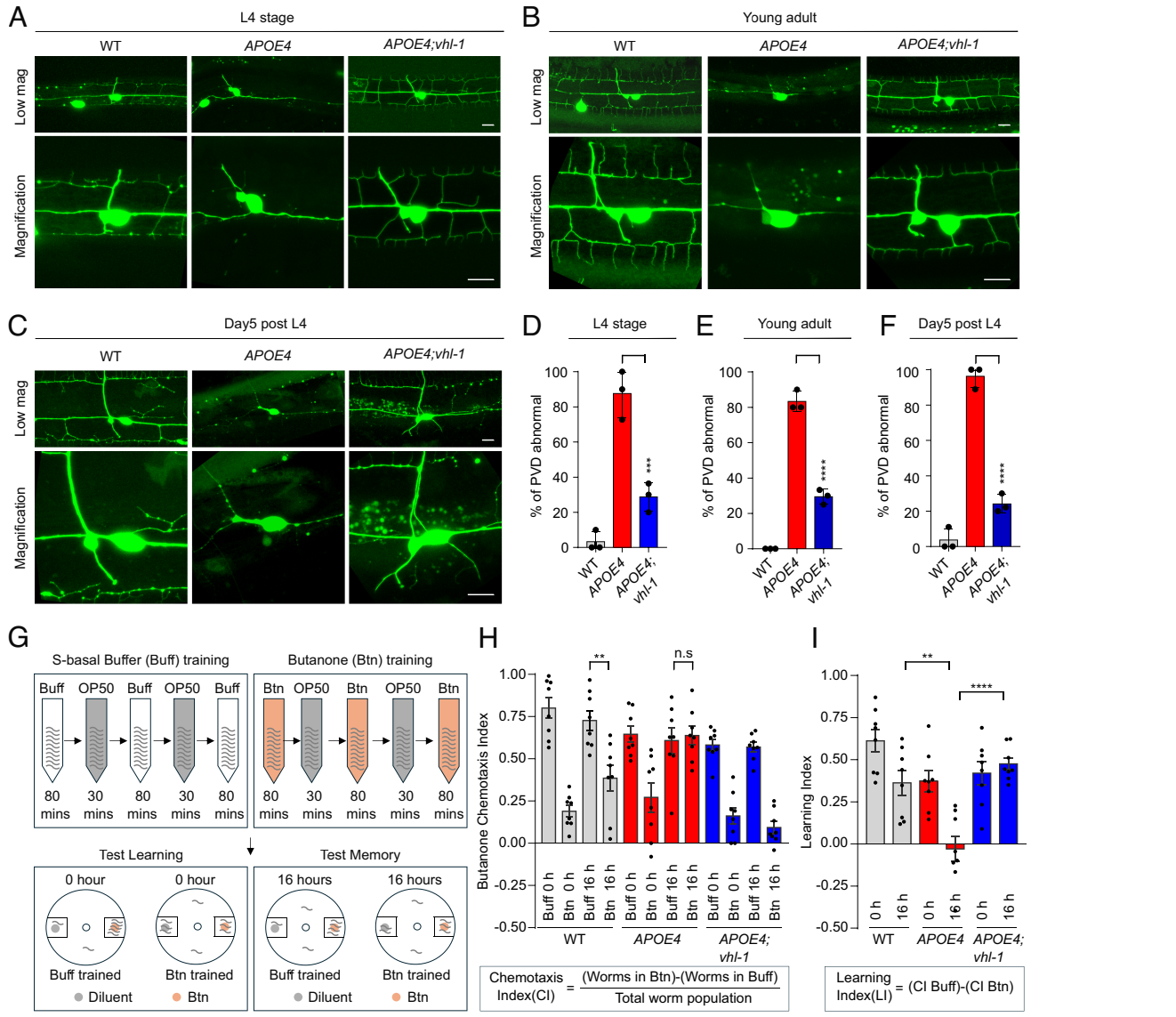

Fig. 4. *APOE4*-induced neuronal and memory defects are restored by *vhl-1*. (*A*) Representative confocal images of PVD neurons in WT, *APOE4(vxIs824)*, and *APOE4(vxIs824); vhl-1(ok161)* at L4 stages on normal NGM showing *vhl-1(ok161)* LOF mutants with rescued APOE4-induced PVD neurons (*wyIs592[ser-2prom-3p::myr-GFP]*) morphological deterioration. (Scale bar: 10 μm.) (*B*) Representative confocal images of PVD neurons in WT, *APOE4(vxIs824)*, and *APOE4(vxIs824); vhl-1(ok161)* at young adult stages on normal NGM showing *vhl-1(ok161)* LOF mutants with rescued APOE4-induced PVD neurons (*wyIs592[ser-2prom-3p::myr-GFP]*) morphological deterioration. (Scale bar: 10 μm.) (*C*) Representative confocal images of PVD neurons in WT, *APOE4(vxIs824)*, and *APOE4(vxIs824); vhl-1(ok161)* at day 5 post-L4 stages on normal NGM showing *vhl-1(ok161)* LOF mutants with rescued APOE4-induced PVD neurons (*wyIs592[ser-2prom-3p::myr-GFP]*) morphological deterioration. (Scale bar: 10 μm.) (*D–F*) Quantification of the percentage of PVD neurons that are abnormal (with the third and fourth branches of PVD neurons missing or severed) in WT, *APOE4(vxIs824)*, and *APOE4(vxIs824); vhl-1(ok161)* under conditions indicated on normal NGM. *** indicates $P < 0.001$ (n > 30 animals per condition). (*G*) Schematic of the assay for training and subsequent analysis. WT, *APOE4(vxIs824), and APOE4(vxIs824); vhl-1(ok161)* at Day 1 old adult worm populations on normal NGM were subjected to repeated, spaced training with either butanone or buffer (control), then split into seconds and tested for learning (chemotaxis assays), placed on plates with food (*Escherichia coli*) for 16 h, and then tested for memory (chemotaxis assays). (*H* and *I*) Learning and 16 h memory. Chemotaxis indices (CIs) and learning indices (LIs) were calculated as indicated. n = 8 trials. **$P < 0.001$, ****$P < 0.0001$, and n.s. indicates nonsignificant.

against these candidate genes to test whether any are functionally important for survival (measured as median lifespan) at 28 °C in both wild type and *vhl-1(ok161)* mutants. We found that genetic deletion or RNAi against each of two candidate genes, *tgn-38* and *Y70C5C.1*, led to increased mortality at 28 °C (Fig. 6 *B–E* and *SI Appendix*, Fig. S7 *A–C*). *tgn-38* encodes a *C. elegans* ortholog of human C5orf15 (chromosome 5 open reading frame 15) and TGOLN2 (trans-golgi network protein 2) with uncharacterized biological functions, whereas *Y70C5C.1* encodes a *C. elegans* ortholog of human IDE (insulin degrading enzyme). Though mechanisms linking TGN-38 to mortality regulation remain unclear, the loss-of-function phenotype of *Y70C5C.1* suggests that HIF-1 may activate expression of an insulin-degrading enzyme, leading to insulin receptor (DAF-2) inhibition and activation of the DAF-16 stress-responding pathway.

Among the most dramatically up-regulated gene by HIF-1 (via stabilized HIF-1 or loss of *vhl-1* at 28 °C), *F22B5.4* encodes a predicted mitochondrial protein [with the probability of mitochondrial presequence of 0.967, mitoFate (59)] of uncharacterized biological function. Although we did not observe the RNAi phenotype of *F22B5.4* (possibly owing to a paralogous gene *F36A2.7* and/or low RNAi efficiency in tissue of expression), single-cell gene expression profiling by CeNGEN indicates its predominant expression in neurons (60). We generated a translational GFP reporter for *F22B5.4* under the control of its endogenous promoter and confirmed its specific expression in neurons (Fig. 6*F*).

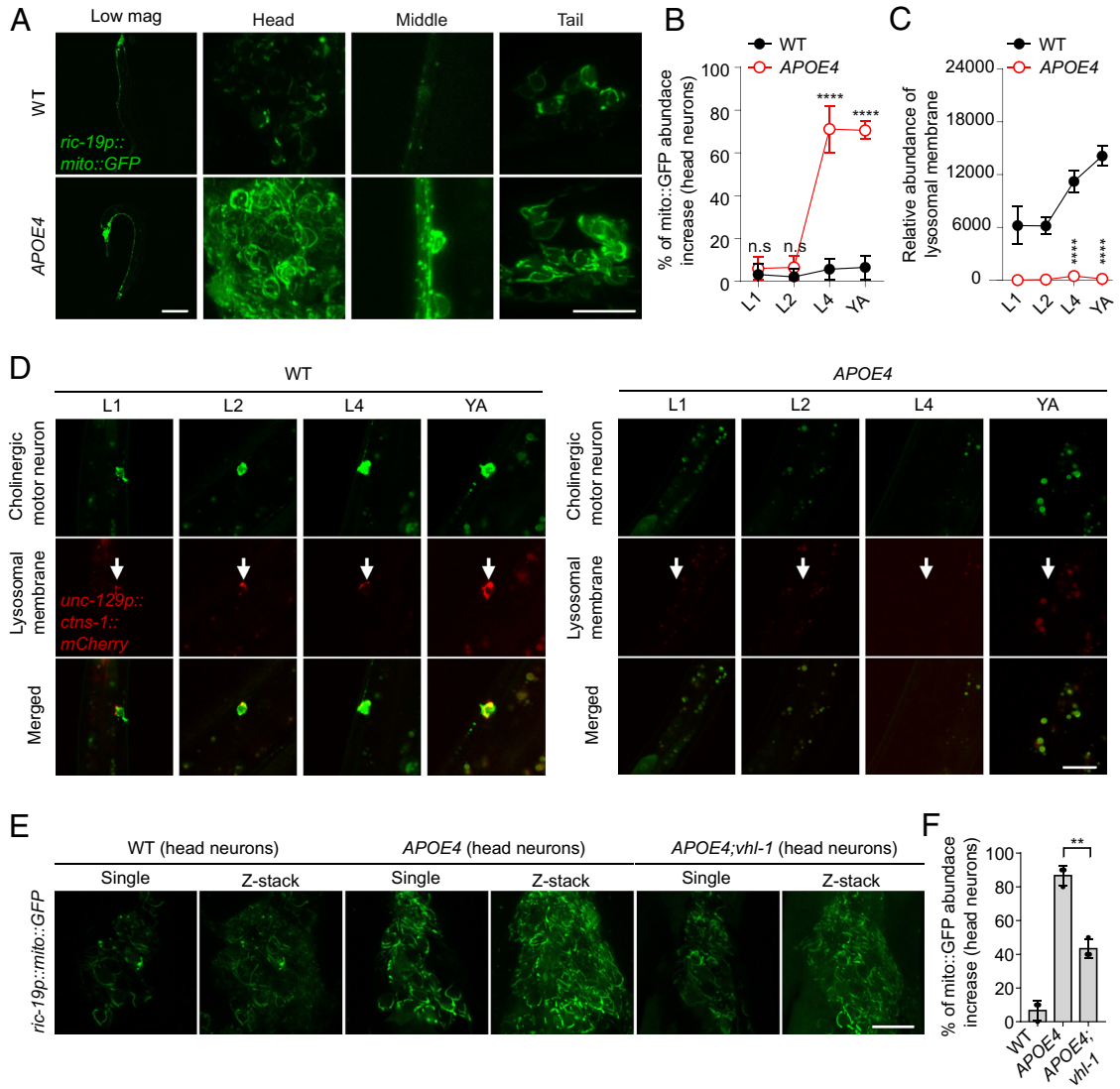

Fig. 5. *APOE4* causes neuronal mitochondrial defects suppressed by *vhl-1*. (*A*) Representative confocal low- and high-magnification images of neuronal tissue-specific expression of the neuronal mitochondria reporter (*ric-19p::mito::GFP*) in WT and *APOE4(vxIs824)* animals at young adult (day 1 post-L4 stages) with indicated position. [Scale bar: 100 μm (low magnification) and 10 μm (high magnification).] (*B*) Quantification of the percentage of neuronal mitochondria reporter (*ric-19p::mito::GFP)* abnormalities based on head neurons in WT and *APOE4(vxIs824)* animals at different stages of L1, L2, L4, and young adult (day 1 post-L4 stages) on normal NGM. **** indicates $P < 0.0001$; n.s. indicates nonsignificant (n > 30 animals per condition). (*C*) Fluorescent quantification of neuronal lysosomal membrane *(unc-129p::ctns-1::mCherry)* in WT and *APOE4 (vxIs824)* animals at different stages of L1, L2, L4, and young adult (day 1 post-L4 stages) on normal NGM. **** indicates $P < 0.0001$ (n > 20 animals per condition). (*D*) Representative confocal images of neuronal lysosomal membrane reporter *(unc-129p::ctns-1::mCherry)* in WT and *APOE4(vxIs824)* at different stages of L1, L2, L4, and Day 1 post-L4 on normal NGM. (Scale bar: 10 μm.) (*E*) Representative confocal images of neuronal mitochondria reporter *(ric-19p::mito::GFP)* in WT, *APOE4(vxIs824)*, and *APOE4(vxIs824); vhl-1(ok161)* at young adult stages with head neuron positions (day 1 post-L4 stages) on normal NGM. (Scale bar: 10 μm.) (*F*) Quantification of the percentage of neuronal mitochondria reporter *(ric-19p::mito::GFP)* abnormalities based on head neurons in WT, *APOE4(vxIs824)*, and *APOE4(vxIs824); vhl-1(ok161)* at young adult stages (day 1 post-L4 stages) on normal NGM. ** indicates $P < 0.01$ (n > 30 animals per condition).

In addition, neuronal-specific gain-of-function of *F22B5.4* by *ric-19* promoter-driven cDNA expression markedly reduced mortality at 28 °C (Fig. 6 *G* and *H*). Neuronal-specific gain-of-function of *F22B5.4* also partially suppressed the mortality phenotype caused by transgenic APOE4 (Fig. 6*I*).

These results identify three previously uncharacterized HIF-1 targets that may functionally contribute to protection of neurons and suppression of animal mortality in *C. elegans*.

Vhl Inactivation Suppresses APOE4-Induced Neurovascular Injuries in Mice. To further evaluate evolutionarily conserved mechanisms by which VHL inactivation may ameliorate toxic effects of APOE4, we assessed the neurovascular injuries in *APOE4* mice (mouse *Apoe* gene was replaced by the human *APOE4* allele by homologous recombination) and the protective action by Vhl inhibition in mice. Human *APOE4* allele replacement in mice can lead to cerebral vascular and blood–brain barrier (BBB) lesions accompanied by compromised tight junctions, and neurodegenerative changes, including synaptic loss (39, 61, 62). To investigate the potential neurovascular benefits of Vhl inactivation in *APOE4* mice, we injected AAV-*Vhl*-shRNA bilaterally into the mouse hippocampus (Fig. 7*A* and *SI Appendix*, Fig. S8*A*). We found that the *APOE4* mice exhibited marked loss of brain capillary pericyte coverage in the hippocampus compared to the WT control (C57BL/6 mice). Inhibition of *Vhl* by shRNA markedly restored pericyte coverage of brain capillaries (Fig. 7 *B* and *C*). We also observed reduced abundance of the tight junction protein, Occludin, in the brains of *APOE4* mice, which was mitigated by *Vhl* inhibition (Fig. 7 *D* and *E*). We assessed the integrity of the BBB by intravenous injection of Evans blue dye

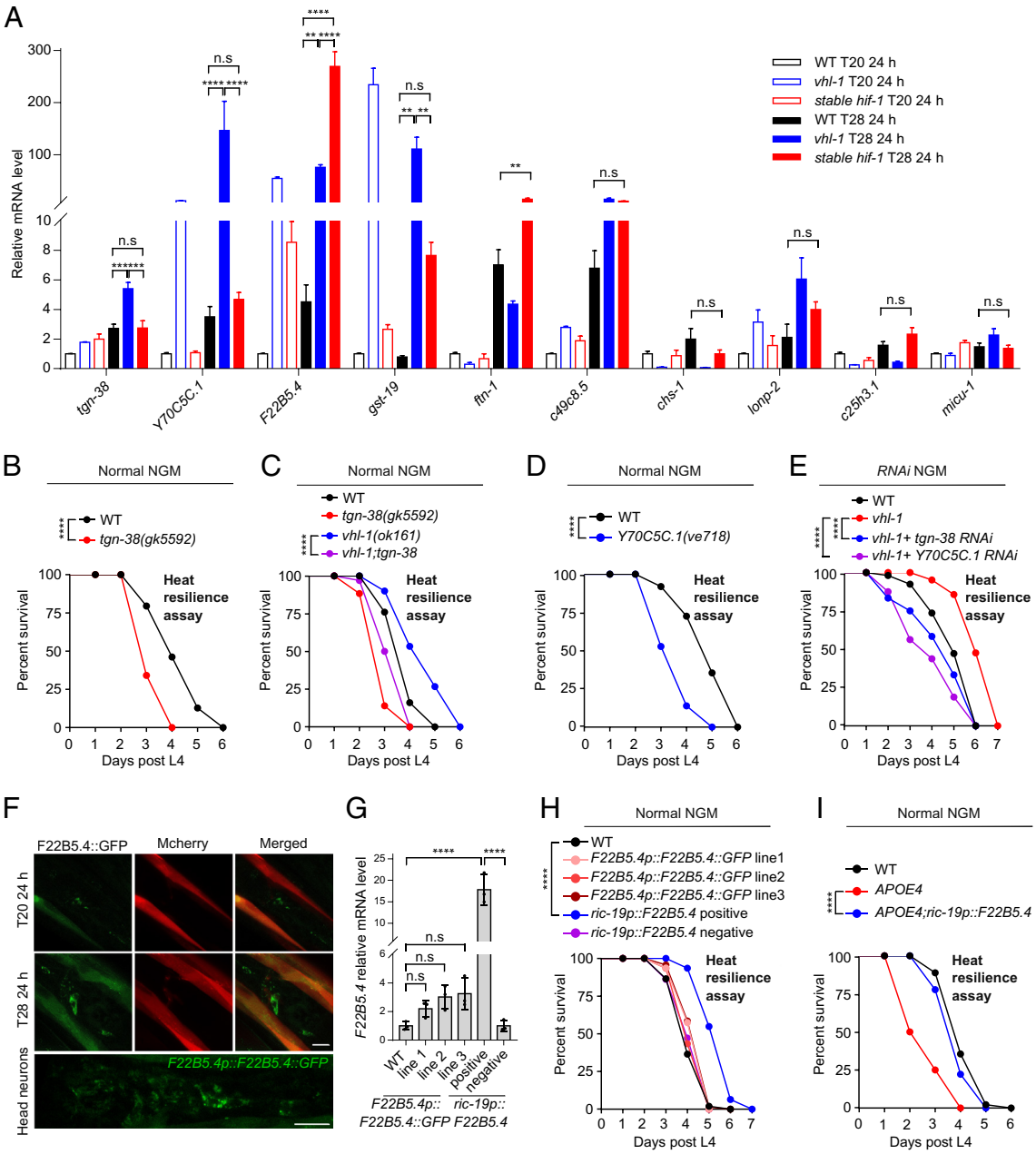

Fig. 6. Characterization of the functional roles of VHL-1/HIF-1 target genes. (*A*) Quantitative RT-PCR measurements of indicated gene expression levels in WT, *vhl-1(ok161)*, and HIF-1 (P621A) *(otIs197)* animals upon sustained treatment at 28 °C or 20 °C for 24 h starting at L4 on normal NGM. ** indicates $P < 0.01$, *** indicates $P < 0.001$, **** indicates $P < 0.0001$, and n.s. indicates nonsignificant. (*B* and *C*) Lifespan curves of WT, *tgn-38(gk5592)* LOF mutants, *vhl-1(ok161)* mutants, and *vhl-1(ok161); tgn-38(gk5592)* double LOF mutants at 28 °C starting at L4 on normal NGM. **** indicates $P < 0.0001$ (n > 40 animals per condition). (*D*) Lifespan curves of WT and *Y70C5C.1(ve718)* LOF mutants at 28 °C starting at L4 on normal NGM. **** indicates $P < 0.0001$ (n > 40 animals per condition). (*E*) Lifespan curves of WT, *vhl-1(ok161) mutants*, *vhl-1(ok161)* mutants with RNAi against *tgn-38* and *Y70C5C.1* at 28 °C starting at L4. **** indicates $P < 0.0001$ (n > 40 animals per condition). (*F*) Representative confocal high-magnification images of the F22B5.4 translational reporter with GFP observed predominantly in head neurons in WT animals. (Scale bar: 10 μm.) (*G*) Quantitative RT-PCR measurements of *F22B5.4* gene expression levels under conditions indicated on normal NGM. **** indicates $P < 0.0001$; n.s. indicates nonsignificant. (*H*) Lifespan curves of WT, three representative F22B5.4 translational reporter lines, and *ric-19p::F22B5.4* overexpression gain-of-function animals at 28 °C starting at L4 on normal NGM. **** indicates $P < 0.0001$ (n > 40 animals per condition). (*I*) Lifespan curves of WT, *APOE4(vxIs824)*, and *APOE4(vxIs824); Ex[ric-19p::F22B5.4, unc-54p::mCherry]* animals at 28 °C starting at L4 on normal NGM. *** indicates $P < 0.001$ (n > 40 animals per condition).

in mice (Fig. 7*F*). Following administration of Evans blue dye, we found that the *APOE4* mice exhibited markedly weakened BBB as evidenced by higher optical density at 620 nm. In contrast, Evans blue content analyses showed that the BBB was largely intact when *Vhl* was knocked down in the brains of *APOE4* mice, reaching levels comparable to those observed in control C57BL/6 mice (Fig. 7*F*). In addition, we observed that *APOE4* caused a marked loss of hippocampal axons and decreased protein levels of the synaptic marker Synaptophysin in the brain, whereas inhibition of *Vhl* markedly reversed both axonal and synaptic degeneration phenotypes caused by *APOE4* (Fig. 7 *G–J*). Collectively, these findings demonstrate that genetic inhibition of *Vhl* can strongly ameliorate *APOE4*-induced cerebrovascular injuries and neuronal synaptic damage in mice.

Discussion

Age-related mortality represents a universal phenomenon influenced by intrinsic genetic factors, environmental stressors, and stochastic events. In this study, we investigated how the VHL–HIF axis

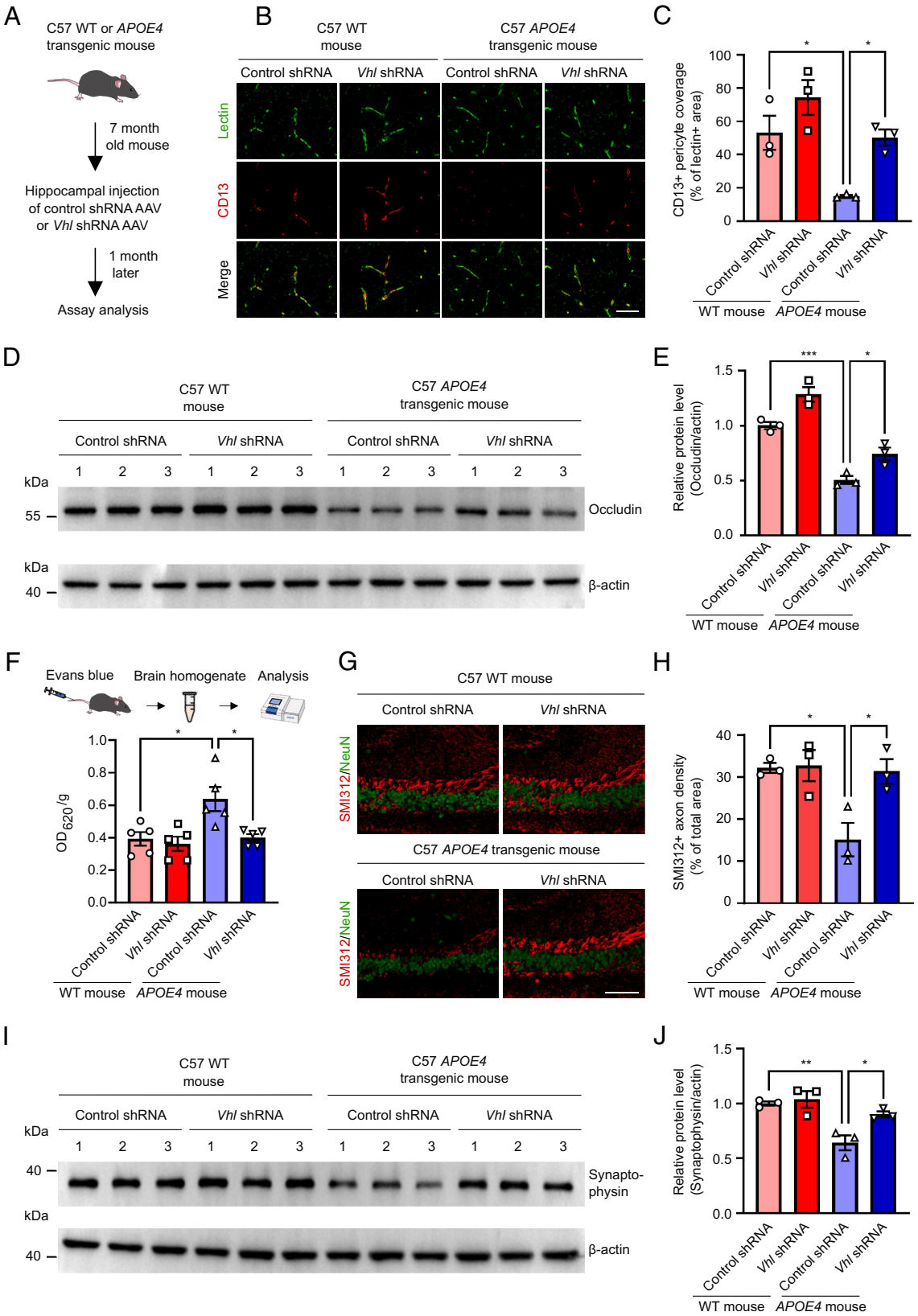

Fig. 7. *Vhl* inhibition mitigates cerebral vascular and synaptic damages in humanized *APOE4* transgenic mice. (*A*) Schematic for the knockdown of *Vhl* by AAV-shRNA in humanized APOE4 transgenic mice. (*B* and *C*) Representative images of CD13+ pericyte coverage (red) of lectin+ endothelial capillary profiles (green) in the hippocampus (*B*). Quantification of pericyte coverage on capillaries (*C*). * indicates $P < 0.05$, n = 3 mice per group. (Scale bar: 50 μm.) (*D* and *E*) Representative western blot showing occludin proteins from mouse brain tissues (*D*) and quantification of relative protein levels of occludin (*E*). * indicates $P < 0.05$; *** indicates $P < 0.001$, n = 3 mice per group. (*F*) Schematic for the Evans blue leakage experiment and quantification of Evans blue leakage in mouse brain tissues. * indicates $P < 0.05$, n = 5 mice per group. (*G* and *H*) Representative images of SMI312+ axons (red) and NeuN+ neurons (green) in the hippocampus (*G*), with quantification of SMI312+ axon density (*H*). * indicates $P < 0.05$, n = 3 mice per group. (Scale bar: 100 μm.) (*I* and *J*) Representative western blot showing synaptophysin proteins from mouse brain tissues (*I*). Quantification of relative protein levels of synaptophysin (*J*). * indicates $P < 0.05$; ** indicates $P < 0.01$, n = 3 mice per group. Data were presented as means ± SEM.

modulates mortality and neural cell damage in *C. elegans* and mice. Our findings reveal that targeting VHL-1 remarkably suppresses mortality induced by various factors, including elevated ROS, temperature stress, and the expression of the human *APOE4* gene variant associated with neurodegeneration and mortality in humans. We established a *C. elegans* model for rapid APOE4-induced neural pathologies and mortality and demonstrated the APOE4 toxicity-suppressing effects of VHL-1 inactivation. We show that stabilized HIF-1 recapitulates the effects of VHL-1 inactivation, likely through orchestrating a genetic program that defends against various cellular dysfunctions linked to mortality, including mitochondrial abnormalities, oxidative stress, proteostasis dysregulation, and endo-lysosomal rupture (*SI Appendix*, Fig. S9). We identified *tgn-38, Y70C5C.1*, and *F22B5.4*, as HIF-1 and VHL-1-regulated genes and possible targets that may functionally contribute to suppression of mortality and neural pathologies.

Extensive studies have investigated mechanisms of cellular toxicity associated with APOE4 in the context of neurodegeneration and AD (63–67). Emerging evidence suggests that neuronal APOE4 may act as a crucial upstream trigger and likely a driver of late-onset AD pathogenesis, leading to downstream neuroinflammation, glial responses, and subsequent neurodegeneration (64). Our study sheds light on the cellular consequences of neuronal APOE4 expression, revealing intrinsic effects of APOE4 in promoting neuronal morphological deterioration, mitochondrial dysfunction, and lysosomal disruption in neurons, but also cross-tissue actions on proteostatic abnormalities in body wall muscles. Neuronal APOE4 may inflict oxidative stress via excess ROS generation and intracellular cholesterol accumulation by multiple mechanisms (63–67), which may separately and additively lead to the observed cellular defects in *C. elegans*. Importantly, reduction of cholesterol from dietary sources or amelioration of excess oxidative stress through NAC or HIF-1 stabilization strongly suppressed these defects, providing a causal link from cholesterol to mortality regulation by VHL–HIF. While hypoxia and oxidative stresses can facilitate AD pathogenesis through cell deleterious effects (ROS generation, energy depletion and redox imbalance, etc.), hypoxia-inducible activation of HIF-1 is primarily adaptive and protective against hypoxic injury and oxidative stress, representing a targetable pathway for alleviation of neurodegeneration in AD.

In mice, we showed that *Vhl* knockdown mitigated neurovascular injuries induced by APOE4. Beneficial effects of targeting Vhl in neural tissues include enhanced pericyte coverage, preservation of tight junction proteins, and protection against BBB compromise and synaptic loss. This evidence of a conserved mechanism in a mammalian system strengthens the potential clinical implications of targeting VHL–HIF for mitigating age-related mortality and neurodegenerative risks associated with APOE4. Although *Vhl* loss or HIF-1 activation in dividing cells could be oncogenic, leading to tumor cell growth, specific targeting of VHL–HIF in nonproliferative tissues, such as postmitotic neurons, might broadly protect against oxidative stress resulting from ischemia–reperfusion injuries, neurodegeneration, aging, or *APOE4* genetic predisposition. The integration of our findings across different species paves the way for future studies into conserved mechanistic links underlying the complex relationships among genetic factors, cellular pathways, and environmental influences on mortality.

Our studies are based on largely genetic, cell biological, and phenotypic analyses, demonstrating causal inferences, yet lacking molecular and biochemical mechanistic details. For example, the precise mechanisms by which the three HIF-1 targets protect against cellular damage and animal mortality in *C. elegans* await further studies. Whole-animal genetic LOF of *vhl-1* and constitutive expression of stabilized HIF-1 preclude high-resolution dissection of the spatiotemporal requirement of VHL–HIF signaling in protection against cellular damages and animal mortality. The proteostasis defects in body wall muscles and morphological deterioration of PVD neurons caused by pan-neuronal expression of *APOE4* raise intriguing cell biological questions regarding mechanisms of cross-tissue interactions, but the relative contribution of cell-autonomous and non-cell-autonomous effects of APOE4 to mortality in *C. elegans* remain undetermined. Although loss of *vhl-1* or HIF-1 activation protects against mortality in *C. elegans*, it remains unclear whether it is also true in mice or humans. In addition, the broader implications of VHL–HIF modulation on other aspects of organismal health and aging, such as behavioral outcomes and healthspan, warrant further investigations.

Materials and Methods

C. elegans, transgenic arrays, compound and confocal imaging, western blotting, immunofluorescence, LTM and chemotaxis assay, RNAi, qRT-PCR, thermal resilience and lifespan assays, miniSOG assay, NAC compound treatment, animal body size assay, cell culture and transfection, lentivirus and cell line generation, mammalian cell thermal resilience assay, mice and AAV injection, and Evans blue leakage experiments are described in detail in *SI Appendix*, *SI Materials and Methods*.

All animal experiments were performed in accordance with the Guide for the Care and Use of Laboratory Animals (Eighth edition). The animal experiments were approved by the Institutional Animal Care and Use Committee of China Pharmaceutical University.

For all representative data, scale bars apply to all panels in a set. All summary graphs show means ± SD unless otherwise specified, with *P* values calculated by unpaired two-tailed *t* tests (comparisons between two groups), one-way ANOVA (comparisons across more than two groups), and two-way ANOVA (interaction between genotype and treatment), with post hoc Tukey and Bonferroni's corrections. The lifespan assay was quantified using Kaplan–Meier lifespan analysis, and *P* values were calculated using the log-rank test. $*P < 0.05$, $**P < 0.01$, $***P < 0.001$, and $****P < 0.0001$.

Data, Materials, and Software Availability. All study data are included in the article and/or *SI Appendix*.

ACKNOWLEDGMENTS. Some strains were provided by the *Caenorhabditis* Genetics Center, which is funded by the NIH Office of Research Infrastructure Programs (P40 OD010440), and by Drs. K. Shen, R. Navarro, and J. Powell-Coffman. We also thank Wormbase.org (NIH grant #U24 HG002223 to P. Sternberg), Wormatlas.org (NIH grant #OD010943 to D.H. Hall), and CenGen (cengen.org) for their immensely helpful resources. The work was supported by NIH grants (R35GM139618 to D.K.M. and RF1AG057355 and R21OD032463 to J.T.P.), Baker Aging Research Institute Investigator Award (D.K.M.), University of California San Francisco (UCSF) Program for Breakthrough New Frontier Research Award (D.K.M.), National Natural Science Foundation of China (No. 82173728, S.C.), UCSF California Institute for Regenerative Medicine Scholars Training Program EDUC4-12812 (W.I.J.), Schmidt Science Fellowship (B.Y.W.), and Cancer Research Irvington postdoctoral fellowship (B.Y.W.).

Author affiliations: [a]Cardiovascular Research Institute, University of California San Francisco, San Francisco, CA 94158; [b]Jiangsu Key Laboratory of Druggability of Biopharmaceuticals, State Key Laboratory of Natural Medicines, School of Life Science and Technology, China Pharmaceutical University, Nanjing 210009, China; [c]Immunology Program, Memorial Sloan Kettering Cancer Center, New York, NY 10065; [d]HHMI, Chevy Chase, MD 20815; [e]Department of Neurology, University of California San Francisco, San Francisco, CA 94158; [f]Department of Neuroscience, The Center for Learning and Memory, Waggoner Center for Alcohol and Addiction Research, Institute of Neuroscience, University of Texas at Austin, Austin, TX 78712; [g]Department of Physiology, University of California San Francisco, San Francisco, CA 94158; and [h]Innovative Genomics Institute, University of California, Berkeley, CA 94720

1. F. Schächter *et al.*, Genetic associations with human longevity at the APOE and ACE loci. *Nat. Genet.* **6**, 29–32 (1994), 10.1038/ng0194-29.
2. W. J. Strittmatter *et al.*, Apolipoprotein E: High-avidity binding to beta-amyloid and increased frequency of type 4 allele in late-onset familial Alzheimer disease. *Proc. Natl. Acad. Sci. U.S.A.* **90**, 1977–1981 (1993), 10.1073/pnas.90.5.1977.
3. E. H. Corder *et al.*, Gene dose of apolipoprotein E type 4 allele and the risk of Alzheimer's disease in late onset families. *Science* **261**, 921–923 (1993), 10.1126/science.8346443.
4. P. Sebastiani *et al.*, APOE alleles and extreme human longevity. *J. Gerontol. A Biol. Sci. Med. Sci.* **74**, 44–51 (2019), 10.1093/gerona/gly174.
5. A. Bejanin *et al.*, Association of Apolipoprotein E ε4 allele with clinical and multimodal biomarker changes of Alzheimer disease in adults with Down syndrome. *JAMA Neurol.* **78**, 937–947 (2021), 10.1001/jamaneurol.2021.1893.
6. C. A. Lemere, E. Head, D. M. Holtzman, APOE ε4 association with cognition and Alzheimer disease biomarkers in Down syndrome–implications for clinical trials and treatments for all. *JAMA Neurol.* **78**, 913–915 (2021), 10.1001/jamaneurol.2021.1649.
7. O. Almkvist, C. Graff, The APOE ε4 allele affects cognitive functions differently in carriers of APP mutations compared to carriers of PSEN1 mutations in autosomal-dominant Alzheimer's disease. *Genes (Basel)* **12**, 1954 (2021), 10.3390/genes12121954.
8. J. Fortea *et al.*, APOE4 homozygozity represents a distinct genetic form of Alzheimer's disease. *Nat. Med.* **30**, 1284–1291 (2024), 10.1038/s41591-024-02931-w.
9. L. G. Fritsche *et al.*, A large genome-wide association study of age-related macular degeneration highlights contributions of rare and common variants. *Nat. Genet.* **48**, 134–143 (2016), 10.1038/ng.3448.
10. G. J. McKay *et al.*, Evidence of association of APOE with age-related macular degeneration: A pooled analysis of 15 studies. *Hum. Mutat.* **32**, 1407–1416 (2011), 10.1002/humu.21577.
11. N. La Cunza *et al.*, Mitochondria-dependent phase separation of disease-relevant proteins drives pathological features of age-related macular degeneration. *JCI Insight* **6**, 142254 (2021), 10.1172/jci.insight.142254.
12. S. Milman, N. Barzilai, Discovering biological mechanisms of exceptional human health span and life span. *Cold Spring Harb. Perspect. Med.* **13**, a041204 (2023), 10.1101/cshperspect.a041204.
13. A. Chemparathy *et al.*, APOE loss-of-function variants: Compatible with longevity and associated with resistance to Alzheimer's disease pathology. *Neuron* **112**, 1110–1116.e5 (2024), 10.1016/j.neuron.2024.01.008.
14. M. Dimitriadi, A. C. Hart, Neurodegenerative disorders: Insights from the nematode Caenorhabditis elegans. *Neurobiol. Dis.* **40**, 4–11 (2010), 10.1016/j.nbd.2010.05.012.
15. M. Markaki, N. Tavernarakis, Modeling human diseases in Caenorhabditis elegans. *Biotechnol. J.* **5**, 1261–1276 (2010), 10.1002/biot.201000183.
16. J. J. H. Liang, I. A. McKinnon, C. H. Rankin, The contribution of C. elegans neurogenetics to understanding neurodegenerative diseases. *J. Neurogenet.* **34**, 527–548 (2020), 10.1080/01677063.2020.1803302.
17. T. Pandey, D. K. Ma, Stress-induced phenoptosis: Mechanistic insights and evolutionary implications. *Biochemistry (Mosc)* **87**, 1504–1511 (2022), 10.1134/S0006297922120082.
18. A. K. Corsi, B. Wightman, M. Chalfie, A transparent window into biology: A primer on Caenorhabditis elegans. *WormBook*, 1–31 (2015), 10.1895/wormbook.1.177.1.
19. E. F. Griffin *et al.*, ApoE-associated modulation of neuroprotection from Aβ-mediated neurodegeneration in transgenic Caenorhabditis elegans. *Dis. Model Mech.* **12**, dmm037218 (2019), 10.1242/dmm.037218.
20. C. J. Kenyon, The genetics of ageing. *Nature* **464**, 504–512 (2010), 10.1038/nature08980.
21. C. E. Finch, G. Ruvkun, The genetics of aging. *Annu. Rev. Genomics Hum. Genet.* **2**, 435–462 (2001), 10.1146/annurev.genom.2.1.435.
22. T. E. Johnson, 25 years after age-1: Genes, interventions and the revolution in aging research. *Exp. Gerontol.* **48**, 640–643 (2013), 10.1016/j.exger.2013.02.023.
23. M. Rodriguez, L. B. Snoek, M. De Bono, J. E. Kammenga, Worms under stress: C. elegans stress response and its relevance to complex human disease and aging. *Trends Genet.* **29**, 367–374 (2013), 10.1016/j.tig.2013.01.010.
24. R. Bar-Ziv *et al.*, Measurements of physiological stress responses in C. elegans. *J. Vis. Exp.* (2020), 10.3791/61001.
25. W. I. Jiang *et al.*, Early-life stress triggers long-lasting organismal resilience and longevity via tetraspanin. *Sci. Adv.* **10**, eadj3880 (2024), 10.1126/sciadv.adj3880.
26. J. R. Cypser, P. Tedesco, T. E. Johnson, Hormesis and aging in Caenorhabditis elegans. *Exp. Gerontol.* **41**, 935–939 (2006), 10.1016/j.exger.2006.09.004.
27. C. Kenyon, J. Chang, E. Gensch, A. Rudner, R. Tabtiang, A C. elegans mutant that lives twice as long as wild type. *Nature* **366**, 461–464 (1993), 10.1038/366461a0.
28. K. D. Kd, H. A. Tissenbaum, Y. Liu, G. Ruvkun, daf-2, an insulin receptor-like gene that regulates longevity and diapause in Caenorhabditis elegans. *Science* **277**, 942 (1997), 10.1126/science.277.5328.942.
29. R. Mehta *et al.*, Proteasomal regulation of the hypoxic response modulates aging in C.elegans. *Science* **324**, 1196–1198 (2009), 10.1126/science.1173507.
30. R.-U. Müller *et al.*, The von Hippel Lindau tumor suppressor limits longevity. *J. Am. Soc. Nephrol.* **20**, 2513–2517 (2009), 10.1681/ASN.2009050497.
31. G. L. Semenza, Hypoxia-inducible factors in physiology and medicine. *Cell* **148**, 399–408 (2012), 10.1016/j.cell.2012.01.021.
32. W. G. Kaelin, P. J. Ratcliffe, Oxygen sensing by metazoans: The central role of the HIF hydroxylase pathway. *Mol. Cell* **30**, 393–402 (2008), 10.1016/j.molcel.2008.04.009.
33. D. K. Ma *et al.*, Cytochrome P450 drives a HIF-regulated behavioral response to reoxygenation by C. elegans. *Science* **341**, 554–558 (2013), 10.1126/science.1235753.
34. W. Sae-Lee *et al.*, APP-induced patterned neurodegeneration is exacerbated by APOE4 in Caenorhabditis elegans. *G3 (Bethesda)* **10**, 2851–2861 (2020), 10.1534/g3.120.401486.
35. M. Treinin *et al.*, HIF-1 is required for heat acclimation in the nematode Caenorhabditis elegans. *Physiol. Genomics* **14**, 17–24 (2003), 10.1152/physiolgenomics.00179.2002.
36. D. S. Yoon, M.-H. Lee, D. S. Cha, Measurement of intracellular ROS in Caenorhabditis elegans using 2′,7′-dichlorodihydrofluorescein diacetate. *Bio Protoc.* **8**, e2774 (2018), 10.21769/BioProtoc.2774.
37. S. Chen, S. Luo, Z. Zhang, D. K. Ma, VHL-1 inactivation and mitochondrial antioxidants rescue *C. elegans* dopaminergic neurodegeneration. *Protein Cell* **10**, 610–614 (2019), 10.1007/s13238-019-0621-4.
38. R. W. Mahley, Central nervous system lipoproteins: ApoE and regulation of cholesterol metabolism. *Arterioscler. Thromb. Vasc. Biol.* **36**, 1305–1315 (2016), 10.1161/ATVBAHA.116.307023.
39. Y. Yamazaki *et al.*, Apolipoprotein E and Alzheimer disease: Pathobiology and targeting strategies. *Nat. Rev. Neurol.* **15**, 501–518 (2019), 10.1038/s41582-019-0228-7.
40. S. Vigne, C. Pot, Implication of oxysterols and phytosterols in aging and human diseases. *Adv. Exp. Med. Biol.* **1440**, 231–260 (2024), 10.1007/978-3-031-43883-7_12.
41. V. Matyash *et al.*, Distribution and transport of cholesterol in Caenorhabditis elegans. *Mol. Biol. Cell* **12**, 1725–1736 (2001), 10.1091/mbc.12.6.1725.
42. S.-I. Oh, J.-K. Park, S.-K. Park, Lifespan extension and increased resistance to environmental stressors by N-acetyl-L-cysteine in Caenorhabditis elegans. *Clinics (Sao Paulo)* **70**, 380–386 (2015), 10.6061/clinics/2015(05)13.
43. D. Desjardins *et al.*, Antioxidants reveal an inverted U-shaped dose-response relationship between reactive oxygen species levels and the rate of aging in Caenorhabditis elegans. *Aging Cell* **16**, 104–112 (2017), 10.1111/acel.12528.
44. J. Zhang *et al.*, A delicate balance between bacterial iron and reactive oxygen species supports optimal C. elegans development. *Cell Host Microbe* **26**, 400–411.e3 (2019), 10.1016/j.chom.2019.07.010.
45. Z. Mirza, A. J. M. Walhout, V. Ambros, A bacterial pathogen induces developmental slowing by high reactive oxygen species and mitochondrial dysfunction in Caenorhabditis elegans. *Cell Rep.* **42**, 113189 (2023), 10.1016/j.celrep.2023.113189.
46. Y. B. Qi, E. J. Garren, X. Shu, R. Y. Tsien, Y. Jin, Photo-inducible cell ablation in Caenorhabditis elegans using the genetically encoded singlet oxygen generating protein miniSOG. *Proc. Natl. Acad. Sci. U.S.A.* **109**, 7499–7504 (2012), 10.1073/pnas.1204096109.
47. S. Xu, A. D. Chisholm, Highly efficient optogenetic cell ablation in C. elegans using membrane-targeted miniSOG. *Sci. Rep.* **6**, 21271 (2016), 10.1038/srep21271.
48. D. K. Ma, R. Vozdek, N. Bhatla, H. R. Horvitz, CYSL-1 interacts with the O2-sensing hydroxylase EGL-9 to promote H2S-modulated hypoxia-induced behavioral plasticity in C. elegans. *Neuron* **73**, 925–940 (2012), 10.1016/j.neuron.2011.12.037.
49. B. Wang *et al.*, Co-opted genes of algal origin protect C. elegans against cyanogenic toxins. *Curr. Biol.* **32**, 4941–4948.e3 (2022), 10.1016/j.cub.2022.09.041.
50. M. W. Budde, M. B. Roth, The response of Caenorhabditis elegans to hydrogen sulfide and hydrogen cyanide. *Genetics* **189**, 521–532 (2011), 10.1534/genetics.111.129841.
51. Y. Zhang, Z. Shao, Z. Zhai, C. Shen, J. A. Powell-Coffman, The HIF-1 hypoxia-inducible factor modulates lifespan in C. elegans. *PLoS One* **4**, e6348 (2009), 10.1371/journal.pone.0006348.
52. I. Topalidou, D. L. Miller, Caenorhabditis elegans HIF-1 is broadly required for survival in hydrogen sulfide. *G3 (Bethesda)* **7**, 3699–3704 (2017), 10.1534/g3.117.300146.
53. J. F. Morley, H. R. Brignull, J. J. Weyers, R. I. Morimoto, The threshold for polyglutamine-expansion protein aggregation and cellular toxicity is dynamic and influenced by aging in Caenorhabditis elegans. *Proc. Natl. Acad. Sci. U.S.A.* **99**, 10417–10422 (2002), 10.1073/pnas.152161099.
54. R. Chandra *et al.*, Sleep is required to consolidate odor memory and remodel olfactory synapses. *Cell* **186**, 2911–2928.e20 (2023), 10.1016/j.cell.2023.05.006.
55. A. L. Kauffman, J. M. Ashraf, M. R. Corces-Zimmerman, J. N. Landis, C. T. Murphy, Insulin signaling and dietary restriction differentially influence the decline of learning and memory with age. *PLoS Biol.* **8**, e1000372 (2010), 10.1371/journal.pbio.1000372.
56. J. A. Powell-Coffman, Hypoxia signaling and resistance in C. elegans. *Trends Endocrinol. Metab.* **21**, 435–440 (2010), 10.1016/j.tem.2010.02.006.
57. R. Esmaillie *et al.*, Activation of hypoxia-inducible factor signaling modulates the RNA protein interactome in Caenorhabditis elegans. *iScience* **22**, 466–476 (2019), 10.1016/j.isci.2019.11.039.
58. M. Vora *et al.*, The hypoxia response pathway promotes PEP carboxykinase and gluconeogenesis in C. elegans. *Nat. Commun.* **13**, 6168 (2022), 10.1038/s41467-022-33849-x.
59. Y. Fukasawa *et al.*, MitoFates: Improved prediction of mitochondrial targeting sequences and their cleavage sites. *Mol. Cell Proteomics* **14**, 1113–1126 (2015), 10.1074/mcp.M114.043083.
60. S. R. Taylor *et al.*, Molecular topography of an entire nervous system. *Cell* **184**, 4329–4347.e23 (2021), 10.1016/j.cell.2021.06.023.
61. R. J. Jackson *et al.*, APOE4 derived from astrocytes leads to blood-brain barrier impairment. *Brain* **145**, 3582–3593 (2022), 10.1093/brain/awab478.
62. O. Liraz, A. Boehm-Cagan, D. M. Michaelson, ApoE4 induces Aβ42, tau, and neuronal pathology in the hippocampus of young targeted replacement apoE4 mice. *Mol. Neurodegener.* **8**, 16 (2013), 10.1186/1750-1326-8-16.
63. J. Tcw *et al.*, Cholesterol and matrisome pathways dysregulated in astrocytes and microglia. *Cell* **185**, 2213–2233.e25 (2022), 10.1016/j.cell.2022.05.017.
64. J. Blumenfeld, O. Yip, M. J. Kim, Y. Huang, Cell type-specific roles of APOE4 in Alzheimer disease. *Nat. Rev. Neurosci.* **25**, 91–110 (2024), 10.1038/s41583-023-00776-9.
65. J. M. Long, D. M. Holtzman, Alzheimer disease: An update on pathobiology and treatment strategies. *Cell* **179**, 312–339 (2019), 10.1016/j.cell.2019.09.001.
66. Y. A. Martens *et al.*, ApoE cascade hypothesis in the pathogenesis of Alzheimer's disease and related dementias. *Neuron* **110**, 1304–1317 (2022), 10.1016/j.neuron.2022.03.004.
67. D. A. Butterfield, M. P. Mattson, Apolipoprotein E and oxidative stress in brain with relevance to Alzheimer's disease. *Neurobiol. Dis.* **138**, 104795 (2020), 10.1016/j.nbd.2020.104795.